THE ASTROPHYSICAL JOURNAL, 420:159–170, 1994 January 1

HIGH-RESOLUTION CONTINUUM AND Brγ IMAGING OBSERVATIONS OF M82

J. E. LARKIN,[1] J. R. GRAHAM,[1,2] K. MATTHEWS,[1] B. T. SOIFER,[1] S. BECKWITH,[3]
T. M. HERBST,[3] AND A. C. QUILLEN[4]

Received 1993 March 11; accepted 1993 July 13

ABSTRACT

We report high angular resolution (~0.″6), broad-band imaging at 1.2 μm (*J* band), 1.6 μm (*H* band), 2.2 μm (*K* band), and 3.7 μm (*L′* band) of the central 110″ × 21″ (1.65 kpc × 0.32 kpc) of the nearby starburst galaxy M82. We also present spectral imaging with 90 km s^{-1} resolution in the Brγ (2.17 μm) hydrogen recombination line covering the central 16″ × 16″ (240 pc × 240 pc) of this edge-on, disk galaxy. The broad-band mosaics reveal two plateaus of emission indicative of an inner disk of stars and perhaps a larger bar structure. Color maps reveal an extinction ridge running along the central kiloparsec which is strongest at the nucleus and on the western side. The dust emission is more symmetric, suggesting that a dust lane is in front of the stellar population to the west of the nucleus, and behind the stars to the east; this is again suggestive of a stellar bar with leading dust lanes. Channel maps and a position-velocity image of the Brγ emission reveal two lobes and are consistent with the interpretation that the ionized gas, and hence, the young massive stars are distributed in a toroid of H II regions surrounding the nucleus.

Subject headings: galaxies: individual (M82) — galaxies: starburst — galaxies: stellar content — galaxies: structure — infrared: galaxies

1. INTRODUCTION

The IrrII/Amorphous galaxy M82 is considered a prime example of a starburst system having $L_{IR} \sim 3 \times 10^{10}\ L_{\odot}$ within the central kpc. At 3.2 Mpc (Tammann & Sandage 1968), M82 is also one of the nearest active galaxies and has been studied extensively in essentially every part of the electromagnetic spectrum. M82 is oriented almost edge on, which leads to very high optical extinction toward the nucleus. With a spatial scale of 16 pc arcsec^{-1}, high spatial resolution studies of M82 offer a unique opportunity to study a starburst system in fine detail.

The cause of the disturbed nature of M82 is not entirely determined, but the most likely source is a tidal interaction with its large neighbor M81. Gottesman & Weliachew (1977) observed a "bridge" of H I emission connecting the two galaxies, which they believed had been stripped from M81. Yun (1992) has used *N*-body simulations involving M82, M81, and NGC 3077 to model the H I distribution and finds that tidal interactions can describe the large-scale flows very well.

The central kiloparsec of M82 is known to be the scene of intense star formation and related activities. Radio observations by Kronberg, Biermann, & Schwab (1985) revealed more than 40 nonthermal radio point sources within 300 pc of M82's nucleus. These have been interpreted as young supernova remnants, implying a supernova rate of ~0.3 supernovae per year (Kronberg & Sramek 1985).

Measurements of the molecular gas, including CO, CS, H I and H_2, show a bilobal structure with a diameter of ~400 pc (25″) (Carlstrom 1988; Lester et al. 1990; Lo et al. 1987; Weliachew, Fomalont, & Greisen 1984). Most authors have interpreted the lobes as the cross sections of a torus of molecular gas with the inner region depleted and ionized by hot, young stars. Infrared observations of the ionized gas (Lester et al. 1990; Waller, Gurwell, & Tamura 1992) have revealed a smaller bilobal structure interior to the molecular component. Radio observations at 3 mm (Carlstrom 1988) are dominated by free-free emission and trace the ionized gas. The 3 mm image, which has much lower resolution than the infrared imaging observations, also shows the ionized component interior to the molecular lobes.

Continuum observations at 2.2 μm (*K* band) have been used by Telesco et al. (1991) to find evidence of a kiloparsec long bar. Models of barred galaxies by Combes & Gerin (1985) show that stellar bars often concentrate material in the core at or within the Inner Lindblad Resonance (ILR) by transferring angular momentum out of the nuclear region. In M82, such a concentration may produce the nuclear starburst which is "eating" its way outward through the molecular material, thereby generating the central ionized regions. The starburst would also produce large-scale winds, further depleting the nuclear region of material. Images in Hα (Lynds & Sandage 1964; McCarthy, Heckman, & van Bruegel 1987; Armus, Heckman, & Miley 1990) have revealed plumes of ionized material well above and below the nucleus of the galaxy consistent with large-scale winds emanating from the nuclear starburst.

For a thorough review of M82 and starbursts in general, readers are directed to the papers by Rieke et al. (1980) and Telesco (1988).

In this paper, we report new, high spatial resolution observations in both the near-infrared continuum and in the Brγ recombination line. The continuum traces stellar light and hot dust emission, while the Brγ recombination line of hydrogen (Brγ 2.165 μm) traces sources of Lyman continuum flux, i.e.,

[1] Palomar Observatory, California Institute of Technology, 320-47, Pasadena, CA 91125.
[2] Alfred P. Sloan Research Fellow. Postal address: University of California, Berkeley, Astronomy Department, 601 Campbell Hall, Berkeley, CA 94720.
[3] Max-Planck-Institut für Astronomie, Königstuhl 17, D-6900 Heidelberg 1, Germany (postal address) and Cornell University.
[4] California Institute of Technology, 130-33, Pasadena, CA 91125.

hot young stars, and therefore locations of current star formation. The dust opacity in the infrared is much lower than at optical wavelengths ($A_{2.2\mu m} \sim 1/10 A_V$) so the Br$\gamma$ and infrared continuum photons can readily escape from regions of comparatively high extinction.

2. OBSERVATIONS AND DATA REDUCTION

2.1. *J, H, and K Continuum Imaging*

M82 was observed with the 5 m Hale telescope of Palomar Observatory on 1988 October 25 using the infrared camera at the Cassegrain f/70 focus. The camera uses a 58 × 62 element InSb array with a scale of 0".313 pixel^{-1} for a total field of 18" × 19". Data were taken in broad band filters at 1.27 μm (J band), 1.65 μm (H band), and 2.20 μm (K band). Images were taken along the plane of the galaxy at ~10" spacings so that each field overlapped with half of the next field. The final K mosaic, consisting of 12 frames, is 400 pixels (125", ~1900 pc) by 70 pixels (22", ~330 pc) when aligned with the plane of the galaxy. The final H and J mosaics, consisting of 10 frames each, are somewhat smaller, 110" by 22". Each exposure in each band consisted of a 10 s on source frame followed by a 10 s off source frame centered 120" north to achieve proper sky subtraction. To ensure accurate positioning, an offset guider was centered on a nearby star throughout the observations. While using the offset guider, the pointing accuracy has been shown to be maintainable at better than 0.1 pixels (0".03) rms (J. R. Graham 1992, private communication).

The first step in processing the data was to correct for nonlinearities in the pixels. Each pixel was corrected independently to better than 0.5%. The sky frames were then subtracted from the appropriate object frames. Dome images in each band were dark subtracted and used as flat fields for the respective images. Airmass corrections were made with the largest relative correction being on the order of 4%. The images were then spatially offset using the offset guider positions and a common sky level determined by matching overlapped regions in each frame. The resulting images were mosaicked to produce the large continuum maps.

Flux calibration was performed using images of the star HD 44612 (Elias et al. 1982) taken before and after the M82 exposures. The stellar images had a FWHM of 0".6 at 1.27 μm, and 0".5 at 1.65 μm, and 2.2 μm. Airmasses for the stellar images were kept below 1.15 so that differential tracking errors were less than 0".2. Comparisons of the airmass corrected stellar images before and after the M82 observations showed that the 1.27 and 2.2 μm fluxes were repeatable to within 1%, and the 1.65 μm fluxes to within 2.5%. A synthetic beam of 5" diameter was centered on the 2.2 μm peak and compared with unpublished, single beam photometry measurements of M82 made by G. Neugebauer and collaborators (private communication). The 5" beam measurements agreed to within 3%.

2.2. *L' Continuum Imaging*

Observations in the 3.7 μm (L' band) filter of M82 were obtained at the 5 m Hale telescope of Palomar Observatory on 1992 December 13 using the Cassegrain Infrared Camera described above. Eighteen images taken along the plane of the galaxy were combined into a mosaic 180 pixels (56", ~850 pc) across and 70 pixels (22", ~330 pc) wide (when aligned with the galactic plane). Each 3.7 μm image consisted of 100 co-added frames on source and 100 co-added frames centered 60" south or north of the source. Each frame was a 0.07 s integration, so the final 3.7 μm images had a total integration time of 7 s each. The images were taken in the early morning twilight and the offset guider, which uses an optical camera, was unusable.

The first step in processing the data was to correct for nonlinearities in the pixels, as described above. The sky frames were then subtracted from the appropriate object frames. The sky frames were also combined and dark current subtracted to make a flat-field image. The images were then spatially offset and scaled to one another by matching overlapped regions in each frame. The positional accuracy of each shifted frame is ~1 pixel (0".313) rms. Most of the frames required little or no relative scaling, and only those images which were consistent with a scale factor of 1.0 were used. The resulting images were mosaicked to produce the large map.

The sky was not clear so single beam, L band (3.5 μm) measurements of M82 made by Rieke et al. (1980) were used to flux calibrate the images. Although this method of calibration makes the absolute magnitudes somewhat uncertain (±0.1 mag), the variation across the mosaicked image is significantly smaller (±0.03 mag). The seeing was estimated to be 0".8 from the L' final mosaic.

2.3. *Fabry-Perot* Brγ *Imaging*

High spatial ($\leq 1''$) and spectral (~90 km s^{-1}) resolution, Brγ images of M82 were obtained on the Hale 200 inch telescope on 1989 April 14, and 15, and 1992 March 23, using a Fabry-Perot Interferometer (Herbst & Beckwith 1988), coupled to the Cassegrain Infrared Camera. The Fabry-Perot was placed directly in the converging f/70 Cassegrain beam. A 1.3% bandpass circular variable filter in the camera provided order isolation.

During the three nights, images were obtained of the central 15" of M82 at 19 distinct velocities, ranging from −500 km s^{-1} to +500 km s^{-1}. During the 1989 April run, each on-source integration was 10 minutes followed by a 10 minute sky frame offset 60" in declination from the source. In 1992 March, each integration and corresponding sky frame was 11 minutes. Each night's observations included K continuum images as well as images at +500 km s^{-1}. No line emission was expected or observed in the high-velocity images, and they were thus used to flux calibrate and align the other spectral scans.

The data were reduced by first subtracting the corresponding sky frames. Flat fields were produced by subtracting bias and dark current frames from the sky frames from each night. All images were then flat-fielded and corrections for airmass were made.

The offset guider, mentioned above, was used with the Fabry-Perot but because the observations covered a significant range in airmass, differential refraction between the guider's optical images of the star and the infrared images of M82 made software registration necessary. Alignment and continuum subtraction of the Fabry-Perot images posed an interesting problem since the core of M82 completely filled the field, and each frame contained substantial Brγ flux. Initial alignment was achieved by maximizing the correlation function of the Fabry-Perot frames with a reference 2.2 μm broad-band image. The alignment was verified by producing a scatter plot of the 2.2 μm image versus the Brγ plus continuum image. In the scatter plot each pixel was represented by a point with abscissa given by the Brγ plus continuum flux and ordinate given by just the continuum (as determined by the 2.2 μm reference image). Pixels which do not have line emission form a straight

line with slope equal to the relative scaling of the two images. Pixels with line emission are displaced to the right and are easily identified. The sharpness of the correlation line is a direct measure of the alignment. The line was fit to determine an accurate and unbiased scaling for each Fabry-Perot image. The scaled images were then continuum subtracted using the reference broad-band image. We estimate the final uncertainty of the Brγ flux densities at 0.17 mJy arcsec^{-2}. This uncertainty is almost entirely due to systematic errors in the continuum subtraction process.

The Fabry-Perot interferometer did not produce iso-velocity images due to different effective plate spacings for different points in the field. Plate curvature and coating imperfections also contribute to small velocity shifts across the array. To correct for this spectral distortion, images of an out of focus argon/krypton arc lamp were interleaved between most M82 images. The interference patterns generated by the lamp line were used to determine the spectral shift in each pixel in each Brγ image to better than 25 km s^{-1} The images were combined into a data cube, and each pixel was shifted to its correct spectral location. The resulting cube contained complete spectra across the Brγ recombination line at $\sim$90 km s^{-1} resolution for each pixel in the Fabry-Perot's field (a total of more than 2000 spectra). In the data cube, each pixel's spectrum was used to produce interpolated intensities at regular velocity intervals so that truly isovelocity images could be produced at any velocity from -500 to 500 km s^{-1}. The integrals of all spectra were used to calculate total line flux images. We estimate the line flux uncertainty to be 6.3×10^{-16} ergs cm^{-2} s^{-1} arcsec^{-2}. This value is primarily due to uncertainties in continuum subtraction and numerical integration. The integrated Brγ flux is always less than 3×10^{-3} times the integrated 2.2 μm emission.

Table 1 shows measurements of the Brγ flux in various size apertures, compared with many of the previous Brγ flux measurements taken from the literature. The present results were made by synthesizing beams of the appropriate size applied to the Fabry-Perot data. These measurements show that the present data compare well with the results of Rieke et al. (1980), who used single beam spectroscopy, and with Waller et al. (1992), who used a lower resolution (1".35 pixels), narrow-band image. The present Brγ data do not extend to a diameter of 30" but are consistent with the work of Willner et al. (1977) who used single-beam narrow-band spectrophotometry. The fluxes measured by Lester et al. (1990), using single beam spectroscopy, and Simon, Simon, & Joyce (1979), who used single beam photometry, are consistent with each other but are a factor of 4–5 above the other measurements. The irregular morphology of the H II regions could be a contributing factor, but at this time, we have no definitive reason for the discrepancy.

TABLE 1

SELECTED Brγ FLUX MEASUREMENTS

APERTURE DIAMETER	OBSERVED FLUX ($\times 10^{-14}$ ergs cm^{-2} s^{-1})		REFERENCE TO PREVIOUS MEASUREMENT
	This Work[a]	Previous Measure	
3".8	5.7 ± 0.7	20 ± 4	1
8	26 ± 3	22 ± 2	2
8	26 ± 3	25 ± 3	3
11	48 ± 6	170 ± 40	4
~15	70 ± 11	...	5
30	...	150	6

[a] Error is primarily systematic from continuum subtraction process.

REFERENCES.—(1) Lester et al. 1990; (2) Rieke et al. 1980; (3) Waller et al. 1992; (4) Simon et al. 1979; (5) Entire field; (6) Willner et al. 1977.

3. RESULTS

3.1. *Continuum Images*

Figures 1*a*, 1*b*, 1*c*, and 1*d* show gray-scale images overlaid with contours of M82 at broad-band wavelengths 3.7 μm (L'), 2.2 μm (K), 1.6 μm (H), and 1.2 μm (J), respectively. In general, the images are very consistent with lower resolution maps made in the past (e.g., Dietz et al. 1986; Telesco et al. 1991; Rieke et al. 1980; Pipher et al. 1987). A strong central peak is evident in the 2.2 μm image. The location of the 2.2 μm peak [R.A. (1950.0): 09^{h}51^{m}43^s.53, Decl. (1950.0): 69°55'00".7], as determined by Dietz et al. (1986), lies within 1" (15 pc) of the dynamical center of M82, as found by Weliachew, Fomalont, & Griesen (1984), and is surrounded by symmetric 2.2 μm emission. We will refer to the 2.2 μm brightness peak as the nucleus in the remainder of the paper. A bright ridge of 2.2 μm emission extends 10" east and west of the nucleus and contains several bright knots of emission. A second major peak, denoted K2 in many other papers (e.g., Dietz et al. 1986), is visible $\sim$9" west of the nucleus in the 1.27, 1.65, and 2.2 μm images and is the end of the ridge of emission in the 3.7 μm image. Several additional knots of emission are resolved along the plane of the galaxy out to 30" on either side of the nucleus. In general, the 2.2 μm image is smoother than the 1.27 and 1.65 μm images suggesting that the shorter wavelength maps suffer more from patchy extinction and that the 2.2 μm image is more representative of the true stellar distribution. The 3.7 μm image is smoother still, but contains a large contribution from dust emission while the 2.2 μm is dominated by stellar photospheric emission (see below). We therefore use the 2.2 μm continuum image as the primary tracer of the starlight.

Figure 2 shows the 2.2 μm continuum along with a 5" (75 pc) wide projected profile along the galactic plane. The 2.2 μm profile clearly shows the nucleus with a surrounding plateau out to a radius of 10" (150 pc) in each direction. A second plateau extends out to 30" (450 pc). This outer plateau was first reported by Telesco et al. (1991) and interpreted as possible evidence for a stellar bar. The sharp drops that mark the ends of the inner plateau are resolved and show a steep fall in intensity over $\sim$1".5–2" (22–30 pc).

3.2. Brγ *Images and Velocity Components*

Figure 3 shows the image of the integrated Brγ flux overlayed with a contour plot of the extinction determined from the four broad-band infrared images as described below. The radio points sources reported by Kronberg, Biermann, & Schwab (1985) are marked with stars, and the 2.2 μm nucleus is marked with a crossed circle. Figure 4 shows nine isovelocity slices of the (continuum subtracted) Brγ data cube (in this and all other velocity references, velocities are relative to the systemic velocity with negative velocities approaching and positive receding). The plane of the galaxy, as determined from the outermost K isophotes, and the 2.2 μm peak are marked. Figures 3 and 4 reveal three major lobes of emission. The smallest lobe, $\sim$1".5 × 1".5 (23 pc × 23 pc) in size, is located just to the north of the galaxy's nucleus as defined by the 2.2 μm continuum, and peaks at the systemic velocity of the nucleus. The 50 km s^{-1} velocity component of this lobe is coincident with an apparent

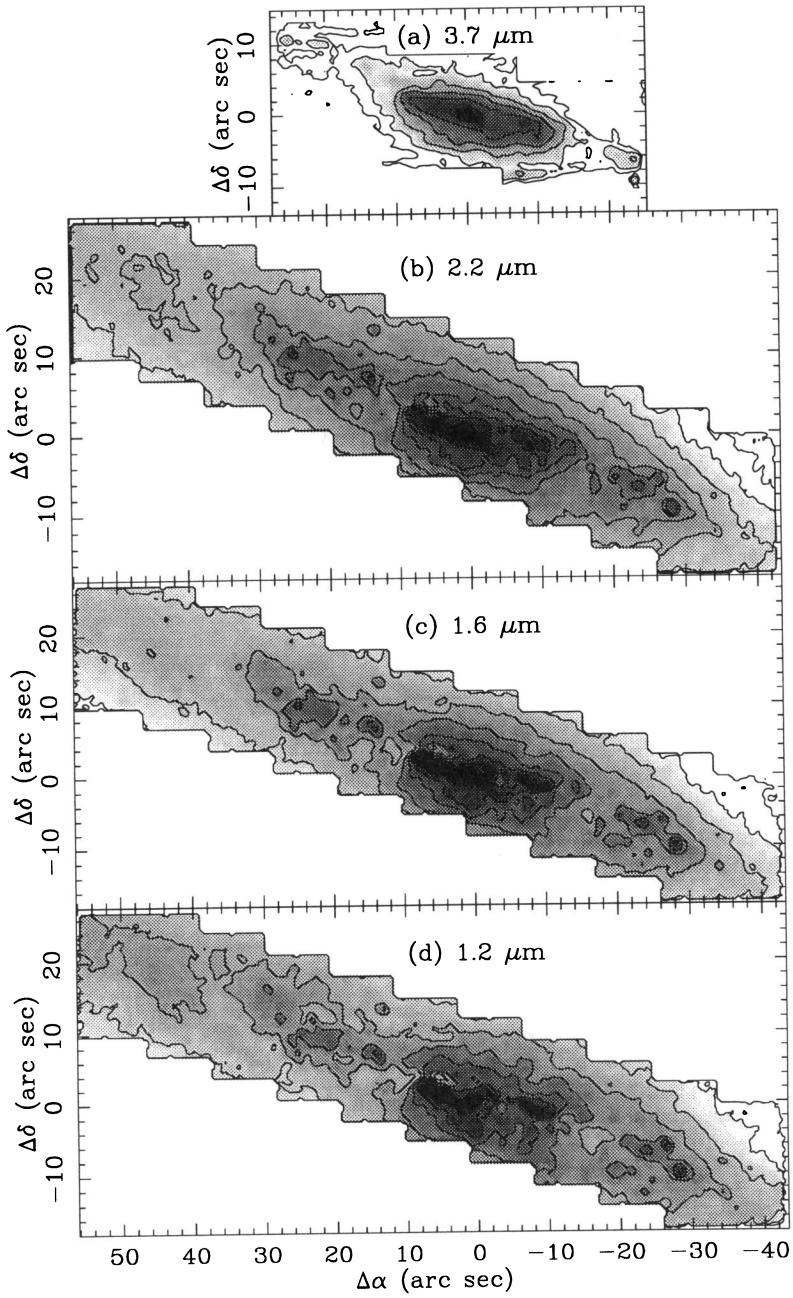

FIG. 1.—Gray-scale plots of the broad-band infrared images with contour overlays: (*a*) 3.7 μm (*L'*) image plotted from 10 (black) to 12.5 (white) mag arcsec^{-2} with contours every 0.5 mag arcsec^{-2}. (*b*) 2.2 μm (*K*) image plotted from 11 (black) to 15.5 (white) mag arcsec^{-2} with contours every 0.5 mag arcsec^{-2}. (*c*) 1.6 μm (*H*) image plotted from 12 (black) to 15.5 (white) mag arcsec^{-2} with contours every 0.5 mag arcsec^{-2}; (*d*) 1.2 μm (*J*) image plotted from 13 (black) to 16.5 (white) mag arcsec^{-2} with contours every 0.5 mag arcsec^{-2}.

"hole" in the *K* emission. This region is ~20 pc across making it comparable in size to a large Galactic H II region. A second much brighter Brγ feature is a large, ~3″ × 3″ (45 pc × 45 pc), emission region located 4″ (60 pc) east of the galaxy's nucleus and centered at ~50 km s^{-1}. This places it ~20 pc below the plane of the galaxy. From the isovelocity images, this eastern region appears to consist of several smaller components. A weak component closer to the plane of the galaxy dominates at high, positive velocity slices (100–150 km s^{-1}). An irregular diffuse component appears to connect the nuclear region and this largest emission region. The diffuse component extends off of the eastern edge of the field. The third major peak is located 4″ west and 3″ south of the galaxy's nucleus. This position, like that of the eastern peak, is below the galaxy's plane. The fact that most of the Brγ flux appears slightly below the plane of the galaxy is probably due to extinction, as evidenced by the extinction overlay in Figure 3 which shows regions of high extinction north of the line emission. The extinction map by Waller et al. (1992) using the [S III] to Hα ratio also shows that the extinction near the nucleus is higher above the plane than below. The western source is close enough to the edge of the Fabry-Perot's field to make its overall size indeterminant. Its shape is more disturbed than the eastern source and a weaker component does extend above the plane of the galaxy and off

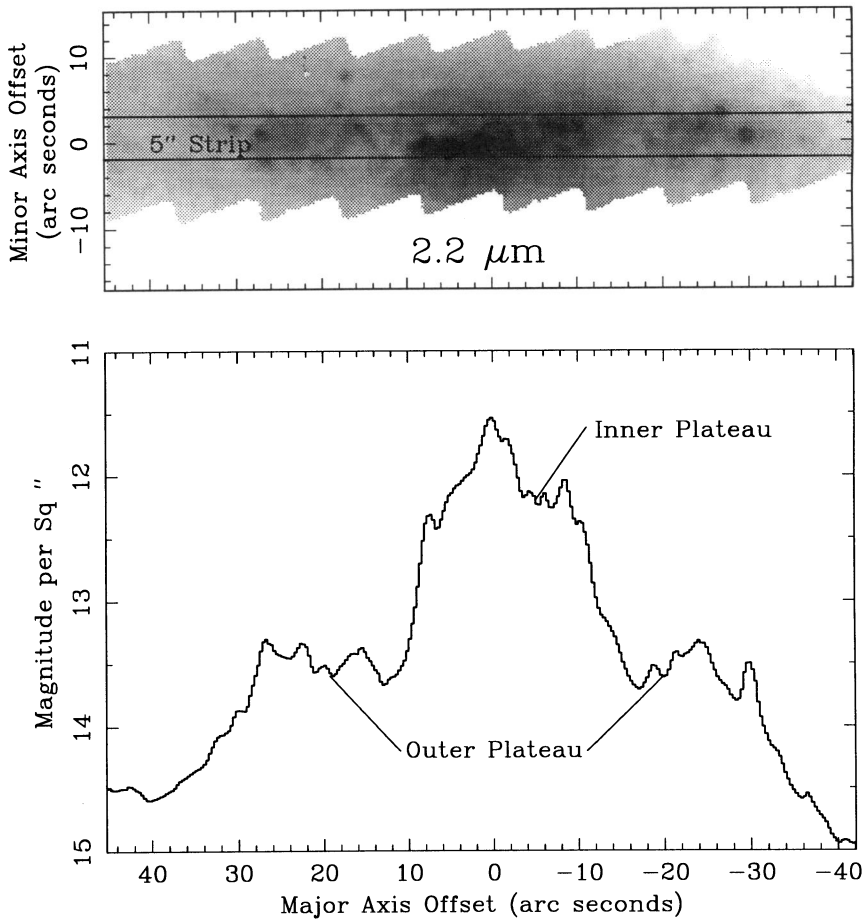

FIG. 2.—A 5″ wide slit is used to generate a 2.2 μm profile along the major axis of the galaxy. Each histogram point is from a 5″ (16 pixel) by 1 pixel rectangle. Note the sharp drops at the ends of the plateaus.

the western edge of the field. Waller et al. (1992) have produced a lower resolution map covering a larger area which shows that both the eastern and western lobes have weaker emission significantly out of the field of view of the present data. Most of the eastern emission and a large fraction of the western lobe lie within the image presented here.

Figure 5 shows a position-velocity map of the Brγ line along the major axis of M82. This plot contains all of the observed Brγ features. The three major lobes discussed above are easily discernible. The curve plotted in Figure 5 is the CO ($J = 1$–0) rotation curve taken from Carlstrom (1988). The CO measurements used a 7″ diameter beam and the rotation curve was therefore based on large-scale features. The rotation curve should not have been sensitive to small-scale structure in the innermost region. It is clear that the Brγ position-velocity map matches the CO rotation curve very well. This shows that the dynamics of the inner ionized region are consistent with those of the outer molecular region, implying that both distributions are created by the same gravitational potential.

Figure 6 shows four position-velocity profiles at different minor axis offsets. The maps show that the Brγ features seen in the integrated map are composed of several different velocity components. Using Figures 4 and 6, a total of more than 10 separate regions can be identified. In the bright eastern source, four separate regions are distinguished. This source has a total extinction corrected (see § 3.4 below) Brγ luminosity of 3.55×10^{38} ergs s^{-1} within a 5″ × 2″.5 box. Assuming case B line ratios, this corresponds to a Lyα flux of $1.14 \times 10^8\ L_\odot$, or $\sim 3 \times 10^7\ L_\odot$ per resolved H II region. This luminosity is an order of magnitude higher than that seen in H II complexes within our own Galaxy (Scoville & Good 1989), even though the individual sources are comparable in size to single H II region clouds. The total flux in the current data is $\sim 70 \times 10^{-14}$ ergs cm^{-2} s^{-1}, which is $\frac{1}{2}$ the flux found in a larger, 30″ beam by Willner et al. (1977). If the number of individual resolved H II regions scales by this same factor, then the entire nuclear region contains ~20 such sources. Using a typical ratio of $L_{IR}/L_{Ly\alpha} \sim 40$ (derived from table in Scoville & Good 1989), the implied L_{IR} is then $2.4 \times 10^{10}\ L_\odot$, as compared to the measured L_{IR} of $\sim 3 \times 10^{10}\ L_\odot$. This is consistent with the infrared luminosity of M82 originating almost entirely within the H II region complexes within 15″ (225 pc) of the nucleus (e.g., Joy et al. 1987; Lester et al. 1990; Rieke et al. 1980; Telesco et al. 1991; Telesco & Harper 1980; Waller et al. 1992). These complexes are vastly more luminous than those seen in our Galaxy.

3.3. *Infrared Colors*

Maps in the infrared colors $J-H$, $H-K$, and $K-L'$ were produced from the four broad-band images (J, H, K, and L'). Figure 7 shows the $J-K$ map. Notice the narrow ridge of large $J-K$ values running along the galactic plane. The eastern side also has a more diffuse component of high $J-K$ color extending significantly out of the plane. These features have been seen

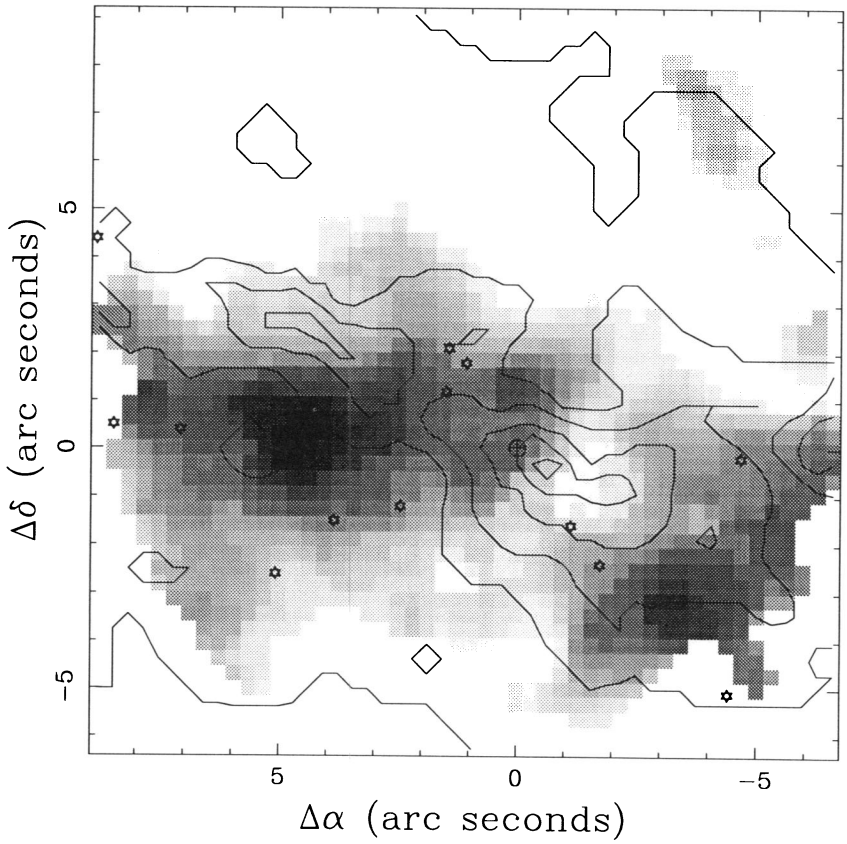

FIG. 3.—Gray-scale image of integrated Brγ emission plotted from 3.5 (white) to 23 (black) ($\times 10^{-16}$ ergs cm^{-2} s^{-1} arcsec^{-2}). Contours of the broad-band extinction are plotted for comparison. Contours are at A_V = 1, 3, 5, 7, 9, and 11 mag. The stars mark the Kronberg, Biermann, & Schwab (1985) nonthermal radio point sources. The circled cross marks the 2.2 μm nucleus. The total field in the image is 16″ × 16″ (240 pc × 240 pc).

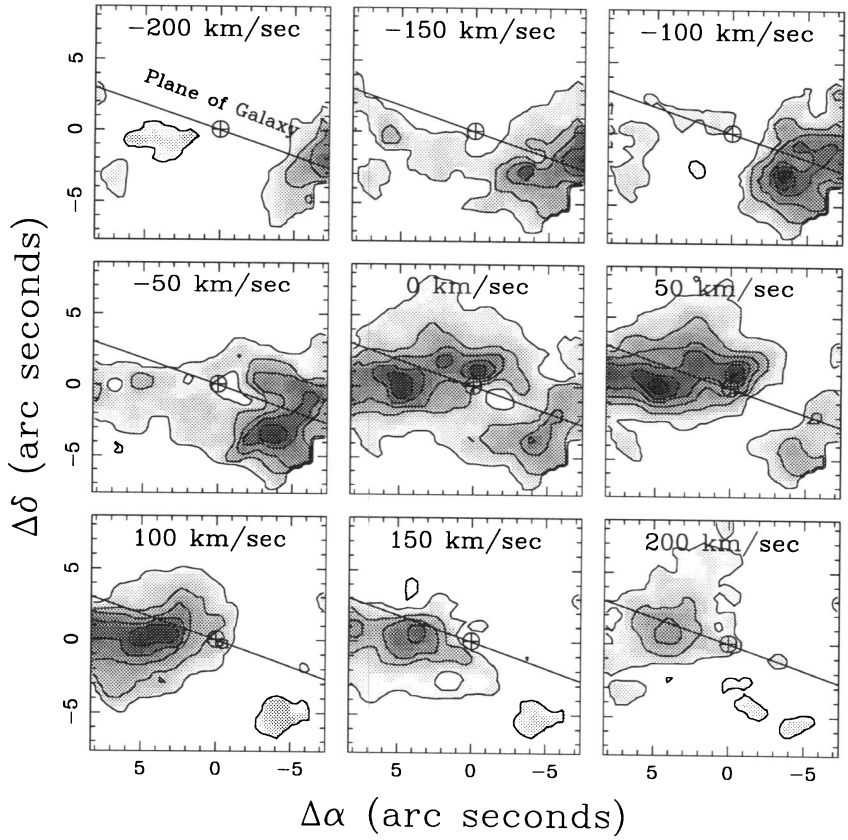

FIG. 4.—Channel maps of the Brγ emission. Each frame is an interpolated isovelocity image of the Brγ flux plotted from 1.0 (white) to 7.5 (black) ($\times 10^{-26}$ ergs cm^{-2} s^{-1} Hz^{-1} arcsec^{-2}), with contours placed every 1.0 × 10^{-26} (ergs cm^{-2} s^{-1} Hz^{-1} arcsec^{-2}). Each frame has a crossed circle to mark the 2.2 μm peak and a line to define the plane of the galaxy.

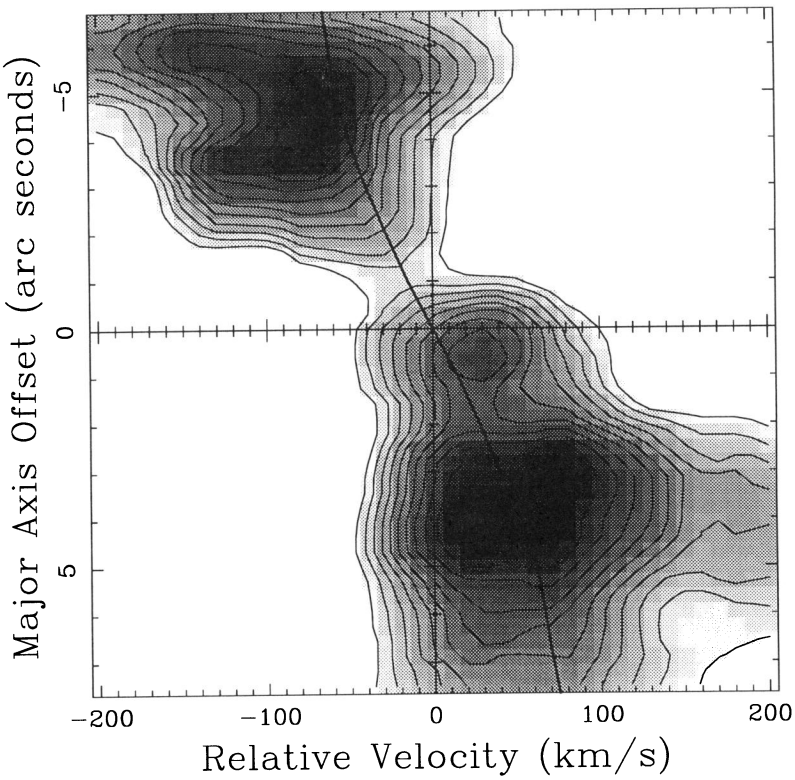

FIG. 5.—Position-velocity map of the Brγ emission integrated over 6″ along the minor axis of the galaxy. The solid curve marks the approximate velocity curve determined by Carlstrom (1988) from CO (1–0) observations over a much larger field. The velocity profiles still include the ~90 km s^{-1} instrumental width. This width increases at the top and bottom of the figure as you approach the edges of the Fabry-Perot.

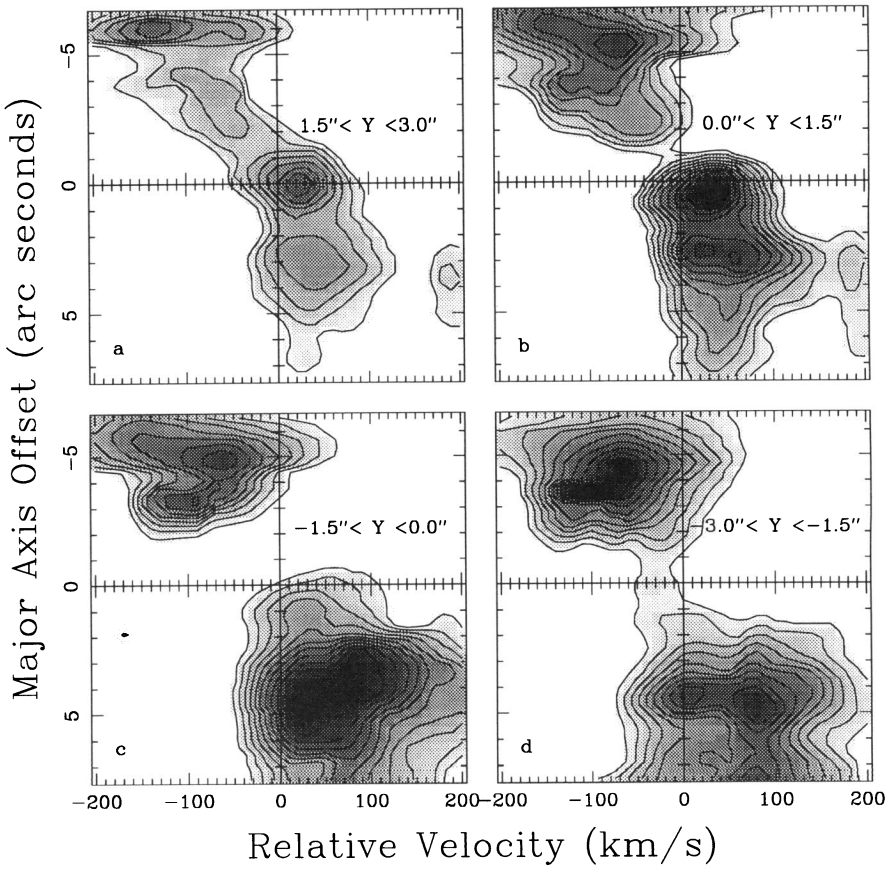

FIG. 6.—Four position-velocity maps similar to Fig. 5. In this case, each frame is over a small range of minor axis offsets. So frame (*a*) is from Brγ emission located 1.″5 to 3.″0 above the plane of the galaxy; (*b*) from emission located 0″ to 1.″5 above the plane; (*c*) from 0″ to 1.″5 below the plane; (*d*) from 1.″5 to 3″ below the plane. Note the many smaller regions which make up the integrated lobes in Fig. 6.

in lower resolution maps by Telesco et al. (1991) and were attributed to extinction from dust. Figure 8 shows a scatter plot of $J-H$ versus $H-K$ values for the entire image. Pixels were binned into 0.″9 squares to represent independent resolution elements. The figure is consistent with a similar plot in Telesco et al. (1991), but we see somewhat greater contamination from dust emission. The figure shows a strong correlation between brighter 2.2 μm continuum flux and redder near infrared colors. The dominant factors in the 1.27, 1.65, and 2.2 μm broad-band colors are emission from stellar photospheres, modest amounts of dust emission ($\sim$10%, although the dust emission does reach fairly high levels in certain localized areas, as shown in § 3.4), and dust extinction (especially along the galactic plane). The uppermost point, at $J-H = 1.9$ mag and $H-K = 1.1$ mag, is roughly centered on the nucleus. Figure 9 shows a similar scatter plot of the $J-H$ versus $K-L'$ colors. Notice the large spread in $K-L'$ colors. This is primarily due to the more significant role that dust emission plays in the 3.7 μm band (L') as compared to the other infrared bands. The lack of an exact L' band calibration does not greatly affect this spread but it does imply an overall uncertainty of $\sim$0.1 mag in the absolute $K-L'$ positioning of the points.

3.4. *Derived Extinctions*

The extinction toward the nucleus and along the narrow ridge of infrared emission has long been a topic of considerable debate (e.g., Lester et al. 1990; Telesco et al. 1991; Waller et al. 1992). Telesco et al. (1991) used J-, H-, and K-band measurements to determine external dust extinction (ignoring dust emission) and found that most of the obscuration was in a symmetric, narrow ridge with $\tau_K \sim 0.5$ ($A_V \sim 5$ mag). Lester et al. (1990) note that using the $J-H$ color and the $H-K$ color separately yields two very different measures of the nuclear extinction ($A_V = 3.7$ and 11.1 mag, respectively), and they conclude that there is significant contamination due to dust emission. Lester et al. (1990) also found from H- and K-band measurements that "the eastern part of the starburst ridge is bluer than the western part," although two broad-band measurements cannot be used to distinguish between dust emission and dust extinction. We believe that the inclusion of the L' image is crucial if one is to separate the effects of dust extinction from dust emission.

As stated above, the significant factors in continuum colors are stellar photospheres, hot ($\sim$1000 K) dust emission from the H II region complexes, and dust extinction. Free-free emission can also play a significant role in infrared colors, but the Brγ image (Fig. 3) and 3 mm image (Carlstrom 1988), show that for M82, free-free emission is always less than 10% of the total broad-brand flux at 2.2 μm, even within the nucleus. If the infrared colors at a given location are due solely to stellar photospheric emission, dust emission at one local temperature and dust extinction from a screen placed between the observer and the stars, then a unique fit of dust temperature, fraction of 2.2 μm flux due to dust, and extinction can be obtained from the four infrared bands J, H, K, and L'. For the fit: intrinsic stellar colors are taken as $J-H = 0.74$, $H-K = 0.2$ (Aaronson 1977), and $K-L' = 0.19$ (Johnson 1966); we allow dust temperatures between 600 and 1000 K; and dust emission is not allowed above 60% of the total K-band flux. Dust emission was modeled by blackbody dust grains with an emissivity $\epsilon \propto \lambda^{-2}$ as done in Aaronson (1977). The extinction law used is from Rieke & Lebofsky (1985). Within the envelope of allowed values, the fit is uniquely defined for all pixels. The fiducial stellar colors were varied by $\pm$0.1 to determine the stability of the fits, and no dramatic deviations were observed. Figure 10 shows the resulting extinction and dust emission maps from the fit with CO (1–0), and 3 mm continuum contours overlaid (Carlstrom 1988). The derived extinction towards the nucleus is $A_V \sim 11$ mag, consistent with most other near-infrared measurements (Telesco et al. 1991, and Lester et al. 1990). The narrow ridge to the west of the nucleus has extinction values ranging from $A_V \sim 4$–6 mag, while the eastern side has relatively low extinction ($A_V \sim 1.5$–3 mag), although it does rise slightly below the plane as one gets closer to the east end of the

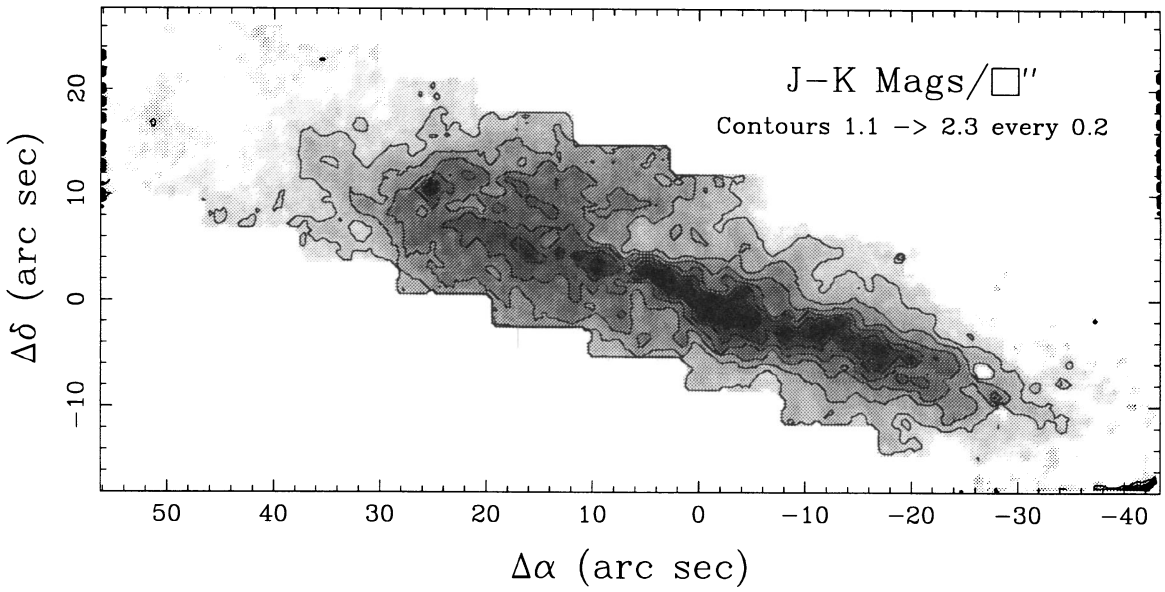

FIG. 7.—The color map generated by subtracting the K magnitude image from the J magnitude image. The gray scale is from $J-K$ of 0.9 (white) to 2.3 (black). Note the high color values along the disk and the diffuse component centered $\sim$20″ east and $\sim$5″ north of the nucleus.

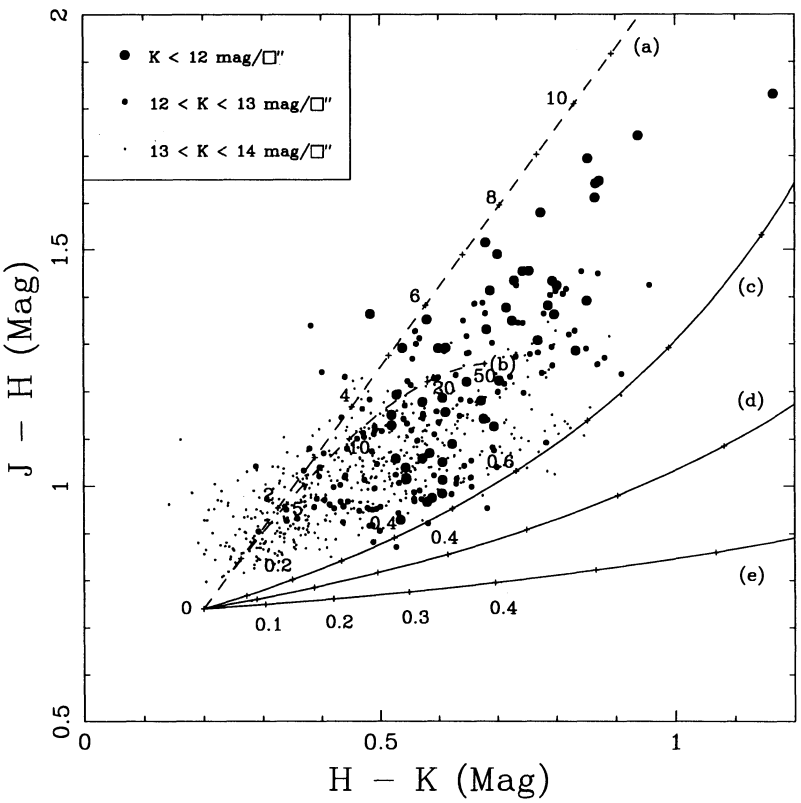

FIG. 8.—Color-color diagram of M82. Each dot corresponds to a 3 pixel by 3 pixel resolution element. The size of the dot is determined by its K magnitude and the position by its $J-H$ and $H-K$ color value. The cross marks the approximate position ($J-H = 0.74$, $H-K = 0.2$) for normal spiral galaxies (Aaronson 1977). Curves represent the effects of various nonstellar processes as determined by calculations similar to Aaronson (1977): (*a*) reddening by a dust screen (labeled in A_V); (*b*) reddening from dust mixed with stars (labeled in A_V); (*c*) emission from 1000 K dust with emissivity $\epsilon \propto \lambda^{-2}$ (labeled by fractional contribution to K); (*d*) same as (*c*) with 800 K dust; (*e*) same as (*c*) with 600 K dust.

bar. This asymmetry is a new result and comes from the inclusion of the L' image and the affect of dust emission. The nonstellar effects to the east are dominated by warm dust emission. Above and below the plane, cooler dust ($\sim$600 K) and low extinction ($A_V \sim 1$ mag) are the only significant effects. The total dust emission within the 2.2 μm band is roughly symmetric about the nucleus, while the extinction is significantly higher to the west. This seems to imply roughly equal amounts of dust on each side with the dust to the west in our line of sight to the stars and thereby producing significant extinction, while the dust to the east lies behind most of the stellar background.

Extinctions were also calculated by comparing the Brγ image with a 6″ resolution, 3 mm image from Carlstrom (1988). Assuming, with Carlstrom, that the 3 mm map is entirely free-free emission (at least at the resolution of his beam), the observed flux density at 3 mm is directly related to the Brγ emission by

$$\frac{F(\mathrm{Br}\gamma)}{10^{-12}\ \mathrm{ergs\ cm^{-2}\ s^{-1}}} = 1.23 \times 10^{-2}\left(\frac{S_{3\,\mathrm{mm}}}{\mathrm{mJy}}\right) \qquad (1)$$

(derived from Condon 1992), where we have assumed an electron temperature of 10^4 K (the temperature dependence of the derived extinction is small). The ratio of this predicted Brγ flux to the measured flux can yield a measure of the extinction. We find an extinction of $A_V \sim 25$ mag at the nucleus, which is significantly higher than that from the broad-band colors. It is not unreasonable that the derived extinction from Brγ is larger than that from the broad band colors, given that the Brγ comes from preferentially dusty regions of higher than average extinction. The smoothing required to match the Brγ image to the 3 mm image also adds uncertainty to the extinctions determined.

An attempt to determine the extinctions from the ratio of Brγ to Hα (obtained from Armus et al. 1990) was also made as in Waller et al. (1992). The obscuration toward the nucleus blocks the Hα so heavily, however, that we do not believe that the two images are representative of the same gas. Once outside the nuclear region, optical emission lines can be a good indicator of the obscuration as evidenced by the [S III]/Hα determination of the extinction by Waller et al. (1992). Lester et al. (1990) use many different line ratios {F([Fe II] 1.257 μm)/F([Fe II] 1.644 μm); hydrogen recombination lines: Hα, Paβ, Brδ, and Brγ} to try and determine the extinction, and find that the nuclear extinctions range from $A_V = 5.4$ at short wavelengths ($\lambda < 2.5$ μm) to $A_V = 15$ at longer wavelengths. This is consistent with the idea that the shorter wavelengths are not seeing all the way to the nucleus and thus measure lower extinctions.

4. DISCUSSION

4.1. *Continuum Morphology (Evidence for a Bar)*

The possible existence of a stellar bar in M82 is not a new idea. The large plateau in the 2.2 μm continuum emission (as seen in Fig. 2) was originally found in a lower resolution map by Telesco et al. (1991) and interpreted as evidence for a bar.

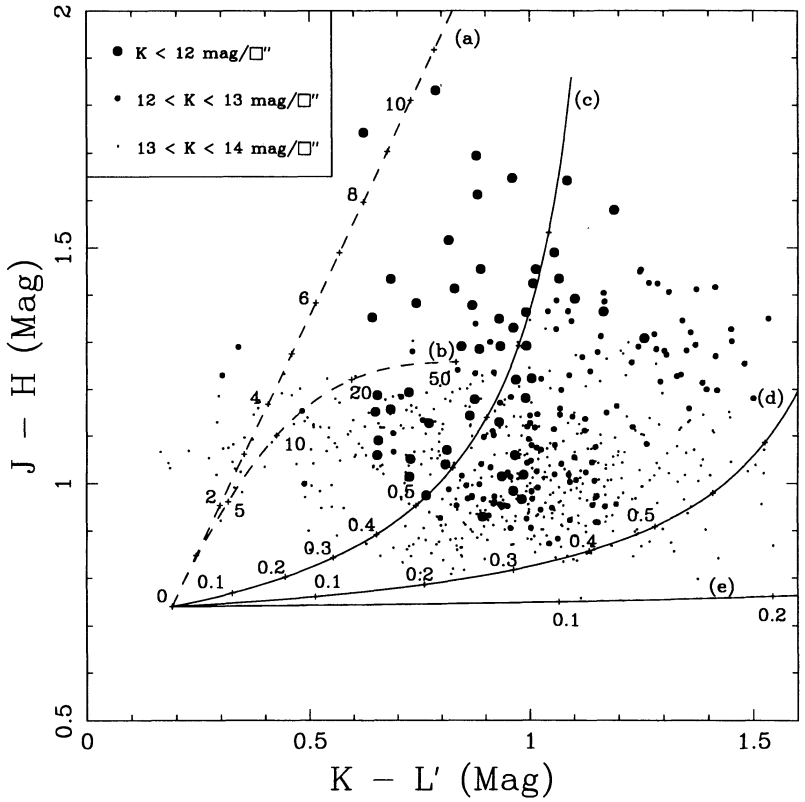

FIG. 9.—Color-color diagram of M82. Each dot corresponds to a 3 pixel × 3 pixel resolution element. The size of the dot is determined by its K magnitude and the position by its $J-H$ and $K-L'$ color value. The cross marks the approximate position ($J-H=0.74$, $K-L'=0.19$) for a normal stellar population (Aaronson 1977; Johnson 1966). Curves represent the effects of various non-stellar processes as determined by calculations similar to Aaronson (1977): (*a*) reddening by a dust screen (labeled in A_V); (*b*) reddening from dust mixed with stars (labeled in A_V); (*c*) emission from 1000 K dust with emissivity $\epsilon \propto \lambda^{-2}$ (labeled by fractional contribution to K); (*d*) same as (*c*) with 800 K dust; (*e*) same as (*c*) with 600 K dust.

They determined a 4° tilt of the plateau's major axis relative to the galaxy's overall orientation and remarked that the rotation is not gradual with increasing flux. The sudden rotation was used to discriminate between a warped disk and a bar morphology, arguing that the tilt was a projection effect that would not be seen in a circularly symmetric feature such as a disk. Beck et al. (1978) found noncircular motions within the plane of M82 and a shear in the velocity contours which they found "qualitatively similar" to that seen in barred spiral galaxies. Beck et al. (1978) suggested that the shear was too pronounced, however, and proposed long lived expulsion of gas by superluminous star clusters to explain the shear velocity. M82 certainly has a great deal of star formation occurring, which could explain the shear velocity, but the plateau and the irregular velocity curve also point to the existence of a bar.

The new result presented here, that the extinction is not symmetric while the dust emission is, gives additional evidence for a stellar bar. The color maps (Fig. 7) show that the regions of high reddening are confined to a thin ridge of obscuring dust on the western side, and a more diffuse region of lower extinction on the eastern side. The asymmetry in the extinction suggests that the dust and the stars cannot be in a simple symmetric disk morphology. The fact that the obscuration is strongest on the side of the galaxy that is rotating toward us implies that there is a dust lane in front of the stellar population there. On the eastern side, which has approximately equal amounts of dust, as evidenced by equal dust emission, the extinction is significantly less, which implies that it is behind most of the stars. So if we could view M82 face-on, we would see the dust confined to two lanes preceding the bar in its rotation about the nucleus. The fact that the extinction also tends to curve above the western end of the bar and increases slightly below the eastern end of the bar is also consistent with preceding dust lanes seen highly inclined. The slight rotation of the dust features also helps to explain why the K-band image is symmetric even though it is more heavily extincted to the west (note that an extinction corrected K-band image still shows the symmetric outer plateau, although the plateau does peak somewhat at the ends). Preceding dust lanes are ubiquitous features of barred systems (e.g., Athanassoula 1992), and their presence within M82 strongly suggests that M82 possesses a bar. A possible face-on view of M82 is presented in Figure 11 and discussed further below.

The strong correlation between the positions of the CO (1–0) lobes (Carlstrom 1988), and the dust features as shown in Figure 10, suggests that they may originate from the same regions within M82. If this is true, and, as argued above, the dust to the east is located behind the stellar bar, then the eastern CO lobe could also originate from a single source behind the bar and is not the limb-brightened edge of a torus. It would then follow that the western CO lobe is also not part of a torus. This alternative picture of the molecular distribution would be of two lobes of gas which are corotating with a stellar bar (The two possible models are shown in Fig. 11). Such bilobal components have been identified in the face-on barred systems M101, NGC 3351, and NGC 6951 (Kenney et

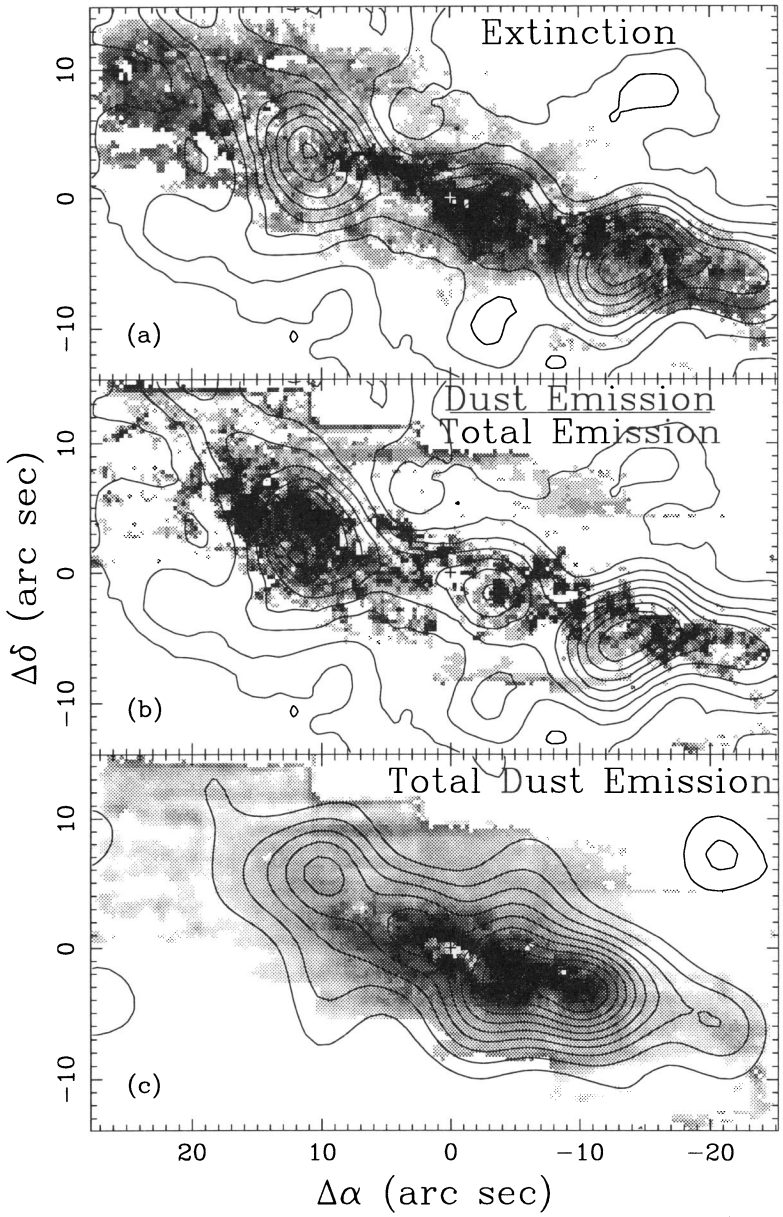

FIG. 10.—The results of fits to the infrared colors for nonstellar effects. (*a*) The extinction in A_V plotted from 1 mag (white) to 5 mag (black). The 2.2 μm peak (marked with a plus) has a derived extinction of $A_V \sim 11$ mag. Carlstrom's (1988) CO (1–0) contours are overlaid for comparison. (*b*) The fraction of hot dust emission at K to the total, extinction-corrected, emission at K, plotted from 0.1 (white) to 0.4 (black). Carlstrom's (1988) CO (1–0) contours are overlaid for comparison. (*c*) The total hot dust emission integrated across all wavelengths, created by using fraction of *K*-band emission and integrating blackbody function at derived dust temperature. Carlstrom's (1988) 3 mm continuum contours are overlaid for comparison. Notice that the hole in the dust emission may be an artifact in the fitting process which has the worst performance at the nucleus due to the extreme colors found there.

al. 1992) and predicted under certain conditions on the angular momentum of the bar by Combes & Gerin (1985). A torus cannot be ruled out, however, since bars can also produce toroids of material interior to the inner Lindblad resonances. Whatever the molecular distribution out of the plane of the sky, the concentration of large amounts of material towards the nucleus is consistent with a stellar bar funneling molecular gas toward the nucleus while angular momentum is transferred outward, thereby fueling the central starburst activity.

4.2. *Emission-Line Morphology*

The two prominent eastern and western Brγ sources are inside the ^{12}CO (1–0) lobes found by Carlstrom (1988). The Brγ sources are roughly coincident with the emission seen at 12.4 μm by Telesco & Gezari (1992) which is consistent with the idea that much of the flux from dust heated in ionized regions is reradiated in the mid-infrared range. The Waller et al. (1992) map shows that on a larger scale, the Brγ emission is still bilobal and highly symmetric. The eastern source is connected by a diffuse component to the nucleus suggesting that the entire eastern side of the inner $\sim 7''$ is filled with ionized gas. A major extinction ridge runs above the eastern source (see Fig. 3) and may obscure much of the Brγ emission in the plane. The western source is only weakly connected to the nucleus, although there again is a region of heavy extinction in this region. The determination that most of the Brγ emission is

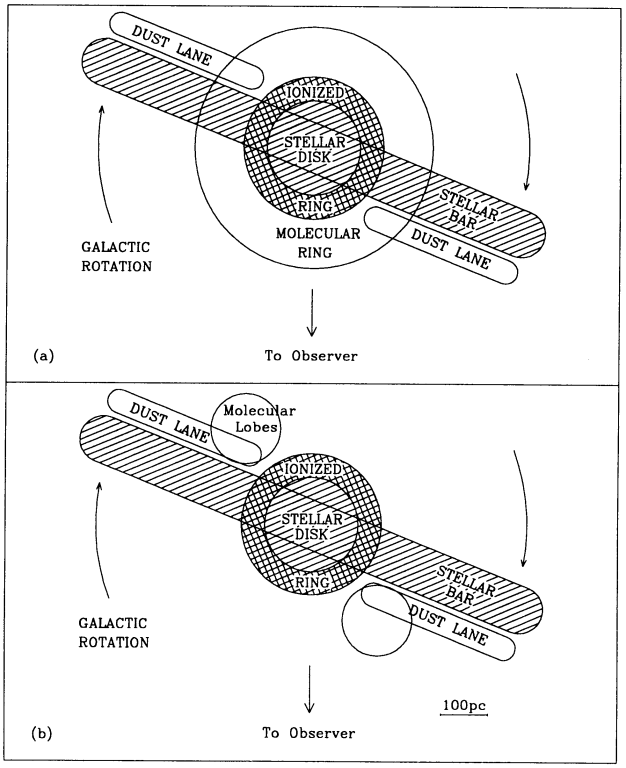

FIG. 11.—Two possible models for the face-on structure of M82. Both models have a stellar bar (single hatch) with a projected length of ~1 kpc with preceding dust lanes. The core has a stellar disk (single and double hatch) which is surrounded by a torus of ionized material (double hatch). Model (*a*) places the molecular component in a ring which is limb brightened, while model (*b*) places the molecular gas in two lobes. The scale is marked for reference, although the models are primarily qualitative in nature.

below the plane of the galaxy has not been seen before and is probably due to the fact that we are viewing M82 from the bottom at a very low inclination angle and the extinction is large in the plane. Telesco (1988) discusses the idea that the center of M82 is filled with Orion-like complexes separated by only a few parsecs and possibly overlapping in some instances.

We have identified 10 distinct H II region complexes within our data cube and from flux comparisons with Willner et al. (1977) estimate the total Brγ flux arises from ~20 such regions. These sources are very compact for their observed luminosities, implying high confinement pressures.

5. SUMMARY AND CONCLUSIONS

We have presented 1.2, 1.6, 2.2, 3.7 μm, and velocity resolved Brγ images along the plane and within the core of M82. The Brγ images of the core are consistent with a ring or perhaps a disk of large, closely spaced H II regions with an overall radius less than 150 pc (10″). The continuum images also make a sudden transition at around 150 pc suggesting that this inner region contains a very bright stellar component. The outer plateau in the continuum emission is ~1 kpc across and very flat. The tight ridge of extinction along the western end of the plateau is consistent with a stellar bar with a preceding dust lane. These observations support and extend the work of Telesco et al. (1991) that suggested that this large plateau is a stellar bar. Observations of the molecular gas (e.g., Carlstrom 1988; Weliachew et al. 1977) have shown that the major molecular features form what could be a limb-brightened torus with an inner radius of 10″ (as shown in Fig. 11*a*). The presence of a bar may imply a truly bilobal distribution of the molecular gas (as shown in Fig. 11*b*) instead of a ring. This possibility is further supported by the spatial correlation of the CO (1–0) lobes and the dust absorption and emission features determined by the infrared continuum colors. The presence of a bar is also consistent with the overall disturbed nature of M82. The tidal interactions of M82 with M81 and NGC 3077 (Yun 1992) could have caused the formation of the bar which now funnels material into the nucleus, thus feeding the starburst and related activity.

The authors are very grateful for enlightening discussions with J. Carlstrom on stellar bars, molecular distributions and dust lanes. We would also like to thank L. Armus, J. Carlstrom, and G. Neugebauer for helpful comments on the paper and access to their data and the anonymous referee for many very helpful suggestions. Special thanks goes to the night assistants at the Hale telescope, Juan Carasco and Skip Staples, and the entire staff of the Palomar Observatory. Infrared astronomy at Caltech is supported by grants from NASA and the NSF.

REFERENCES

Aaronson, M. 1977, Ph.D. thesis, Harvard University
Athanassoula, E. 1992, MNRAS, 259, 345
Armus, L., Heckman, T. M., & Miley, G. K. 1990, ApJ, 364, 471
Beck, S. C., Lacy, J. H., Bass, F., & Townes, C. H. 1978, ApJ, 226, 545
Carlstrom, J. E. 1988, Ph.D. thesis, University of California, Berkeley
Combes, F., & Gerin, M. 1985, A&A, 150, 327
Condon, J. J. 1992, ARA&A, 30, 575
Dietz, R. D., Smith, J., Hackwell, J. A., Gehrz, R. D., & Grasdalen, G. L. 1986, AJ, 91, 758
Elias, J. H., Frogel, J. A., Matthews, K., & Neugebauer, G. 1982, AJ, 87, 1029
Gottesman, S. T., & Weliachew, L. 1977, ApJ, 211, 47
Herbst, T. M., & Beckwith, S. 1988, PASP, 100, 635
Johnson, H. L. 1966, ApJ, 143, 187
Joy, M., Lester, D. F., & Harvey, P. M. 1987, ApJ, 319, 314
Kenney, D. P., Wilson, C. D., Scoville, N. Z., Devereux, N. A., & Young, J. S. 1992, ApJ, 395, L79
Kronberg, P. P., Biermann, P., & Schwab, F. R. 1985, ApJ, 291, 693
Kronberg, P. P., & Sramek, R. A. 1985, Science, 227, 28
Lester, D. F., Carr, J. S., Joy, M., & Gaffney, N. 1990, ApJ, 352, 544
Lo, K. Y., Cheung, K. W., Masson, C. R., Phillips, T. G., Scott, S. L., & Woody, D. P. 1987, ApJ, 312, 574
Lynds, C. R., & Sandage, A. R. 1963, ApJ, 137, 1005
McCarthy, P. J., Heckman, T. M., & van Bruegel, W. 1987, AJ, 93, 264
Pipher, J. L., Moneti, A., Forrest, W. J., Woodward, C. E., & Shure, M. A. 1989, in Proc. Workshop on Ground-based Astronomical Observations with Infrared Detectors, ed. C. G. Wynn Williams & E. E. Becklin (Honolulu: Univ of Hawaii), 326
Rieke, G. H., & Lebofsky, M. J. 1985, ApJ, 288, 618
Rieke, G. H., Lebofsky, M. J., Thompson, R. I., Low, F. J., & Tokunaga, A. T. 1980, ApJ 238, 24
Scoville, N. Z., & Good, J. C. 1989, ApJ, 339, 149
Simon, M., Simon, T., & Joyce, R. R. 1979, ApJ, 227, 64
Tammann, G. A., & Sandage, A. R. 1968, ApJ, 151, 825
Telesco, C. M. 1988, ARA&A, 26, 343
Telesco, C. M., Campins, M., Joy, M., Dietz, K., & Decher, R. 1991, ApJ, 369, 135
Telesco, C. M., & Gezari, D. Y. 1992, ApJ, 395, 461
Telesco, C. M., & Harper, D. A. 1980, ApJ, 235, 392
Waller, W. H., Gurwell, M., & Tamura, M. 1992, AJ, 104, 63
Weliachew, L., Fomalont, E. B., & Griesen, E. W. 1984, A&A, 137, 335
Willner, S. P., Soifer, B. T., Russell, R. W., Joyce, R. R., & Gillett, F. C. 1977, ApJ, 217, L121
Yun, M. S. 1992, Ph.D. thesis, Harvard University